Earth and Planetary Science Letters 451 (2016) 108–113

Contents lists available at ScienceDirect

Earth and Planetary Science Letters

www.elsevier.com/locate/epsl

Estimates of fault strength from the Variscan foreland of the northern UK

Alex Copley [a,*], Nigel Woodcock [b]

[a] COMET, Bullard Labs, Department of Earth Sciences, University of Cambridge, Cambridge, UK
[b] Department of Earth Sciences, University of Cambridge, Cambridge, UK

ARTICLE INFO

Article history:
Received 17 May 2016
Received in revised form 12 July 2016
Accepted 13 July 2016
Available online xxxx
Editor: P. Shearer

Keywords:
fault strength
Variscan
seismogenic thickness

ABSTRACT

We provide new insights into the long-standing debate regarding fault strength, by studying structures active in the late Carboniferous in the foreland of the Variscan Mountain range in the northern UK. We describe a method to estimate the seismogenic thickness for ancient deformation zones, at the time they were active, based upon the geometry of fault-bounded extensional basins. We then perform calculations to estimate the forces exerted between mountain ranges and their adjacent lowlands in the presence of thermal and compositional effects on the density. We combine these methods to calculate an upper bound on the stresses that could be supported by faults in the Variscan foreland before they began to slip. We find the faults had a low effective coefficient of friction (i.e. 0.02–0.24), and that the reactivated pre-existing faults were at least 30% weaker than unfaulted rock. These results show structural inheritance to be important, and suggest that the faults had a low intrinsic coefficient of friction, high pore-fluid pressures, or both.

1. Introduction

The rheology of active faults is a major source of debate. A general issue concerns the magnitude of stresses that faults can support before breaking in earthquakes, or undergoing creep at a significant rate. Previous studies have used a range of techniques to address this question, and have obtained a range of different results. The debate has often focused on estimating the coefficient of friction of faults (either the intrinsic value, or the effective coefficient of friction resulting from the combination of rock properties and pore fluid pressures). Hydro-fracturing in boreholes has been used to infer that the crust is cut by faults with an intrinsic coefficient of friction similar to that suggested by 'Byerlee's Law' (i.e. ∼0.6–0.8; Byerlee, 1978), and hydrostatic pore-fluid pressures (e.g. Brudy et al., 1997; Townend and Zoback, 2000). In contrast, some experiments on fault rocks cored by boreholes have resulted in much lower estimates of the intrinsic coefficient of friction (i.e. ≤0.3; Lockner et al., e.g. 2011; Ujiie et al., e.g. 2013). Geophysical arguments have been made that imply similarly low effective coefficients of friction (e.g. Lamb, 2006; Copley et al., 2011). The distribution of earthquake nodal plane dips has been interpreted as evidence for both high intrinsic coefficients of friction (e.g. ∼0.6; Sibson and Xie, 1998; Collettini and Sibson, 2001), and also as an indicator of intrinsically low friction on fault planes (e.g. ≤0.3; Middleton and Copley, 2014; Craig et al., 2014). The resolution of this debate has important implications for our understanding of lithosphere rheology, and also for assessing earthquake hazard. If fault friction is low, then earthquake stress-drops (commonly in the range of megapascals to tens of megapascals (e.g. Kanamori and Anderson, 1975; Allmann and Shearer, 2009) are likely to represent the majority of the pre-earthquake shear stress on the fault plane, and significant time for stress build-up will be required before earthquakes can nucleate again on a ruptured section of fault. If fault friction is high, then stress-drops in earthquakes will be only partial, and the timing of subsequent ruptures on a given fault could be highly variable. In view of the uncertainty regarding fault friction, this study aims to provide new information by studying the late Carboniferous deformation in the northern UK, in the foreland of the Variscan Mountain range. As part of this work, we outline how to estimate the seismogenic thickness in ancient deformation zones at the time they were active (by using a scaling between seismogenic thickness and basin geometry), and describe a method to calculate the force exerted between mountain ranges and their adjacent lowlands that takes into account thermal structures and chemical depletion.

* Corresponding author.
E-mail address: acc41@cam.ac.uk (A. Copley).

http://dx.doi.org/10.1016/j.epsl.2016.07.024
0012-821X/

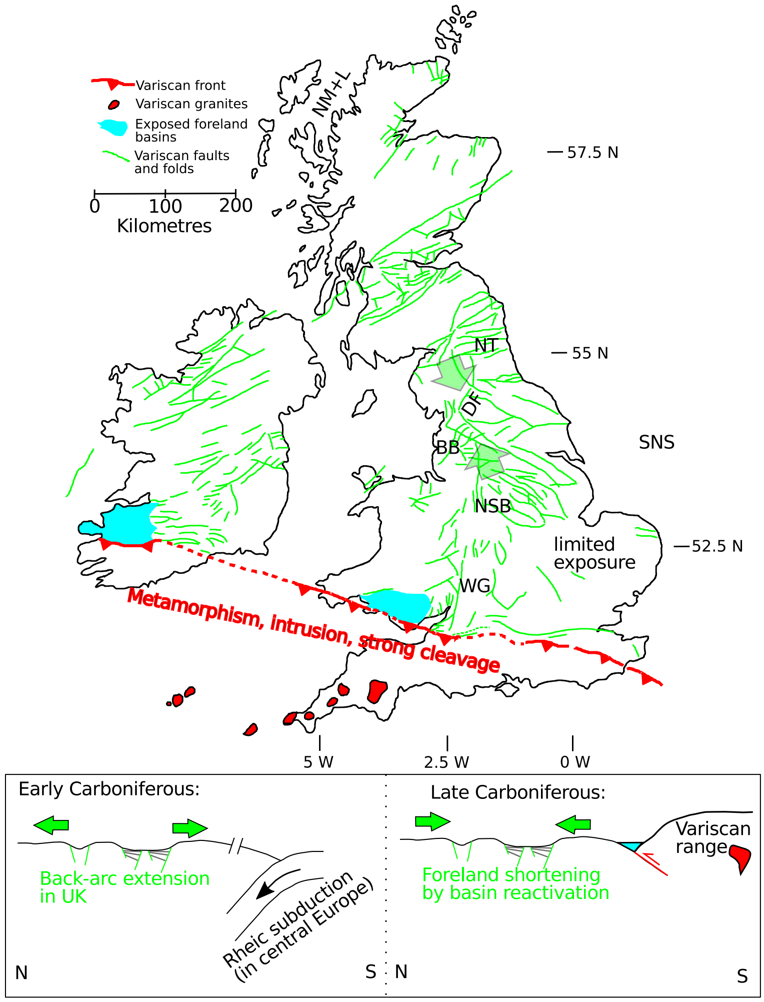

Fig. 1. Summary of Variscan tectonics of the UK, adapted from Warr (2012), after British Geological Survey (1996). Metamorphism and intrusion occurred in the region to the south of the red line, which marks the Variscan range-front. Blue shading shows exposed areas of the Variscan foreland basin. Green lines show faults and folds that were active in the foreland of the Variscan mountain range. The green arrows in the centre of the map show the regional shortening direction estimated by Woodcock and Rickards (2003). DF denotes the Dent Fault. Other black labels show the locations of Carboniferous and Permian–Triassic extensional basins mentioned in the text. NM + L: North Minch and North Lewis Basins; NT: Northumberland Trough; BB: Bowland Basin; NSB: North Staffordshire Basin; WG: Worcester Graben; SNS: Southern North Sea. The lower diagrams show schematic cross-sections during early and late carboniferous times. (For interpretation of the references to colour in this figure legend, the reader is referred to the web version of this article.)

2. The Variscan Foreland of the northern UK

The Variscan Mountain range formed due to the collision between Gondwana and Laurussia, reached its maximum intensity in the late Carboniferous, and produced a Tibetan-scale orogenic belt covering central/southern Europe, and parts of northern Africa and North America. The range front of the northern margin of the Variscan Orogenic belt was just within the southern UK (Fig. 1). Immediately south of this line, the Variscan Orogeny involved folding, cleavage formation, and low-grade metamorphism of sedimentary rocks (e.g. Woodcock and Strachan, 2012, and references therein). The metamorphic grade increases southwards into northern France, and late-orogenic granites are common. Flexural foreland basin deposits are exposed in some locations, immediately to the north of the Variscan front (shown in blue on Fig. 1). North of this flexural basin, many compressional structures were active in the foreland of the mountain range (e.g. Corfield et al., 1996; Warr, 2012). These faults and folds, most of which reactivate pre-existing features, commonly underwent displacements of hundreds of metres to 1–2 km (e.g. Corfield et al., 1996; Woodcock and Rickards, 2003; Warr, 2012; Thomas and Woodcock, 2015). The deformation is analogous to the shortening observed in the forelands of modern orogenic belts, which occurs in response to the compressive force exerted between the mountains and the adjacent lowlands (e.g. in the Himalayan foreland of India (e.g. Copley et al., 2011) and the Andean foreland of South America (e.g. Assumpcao, 1992)). In this paper we estimate an upper bound on the shear stresses required to make faults slip in the Variscan foreland, by resolving the total force exerted between the mountains and the lowlands onto the seismogenic layer in the region. This estimate is an upper bound for the stresses that were required to cause fault slip, because some of the total force could have been supported by the ductile lithosphere. Our calculations lead to insights into fault strength in addition to what has so far been achieved in the equivalent modern settings because of the detailed geological mapping that has been undertaken in the northern UK, which allows the geometry of the structures to be estimated.

3. Scaling between seismogenic thickness and extensional basin width

In order to estimate the seismogenic thickness during the late Carboniferous in the northern UK it is necessary to construct a method to infer this value from present-day observables. Previous studies have documented that the maximum widths of extensional basins bounded by normal faults are related to the depth extent of

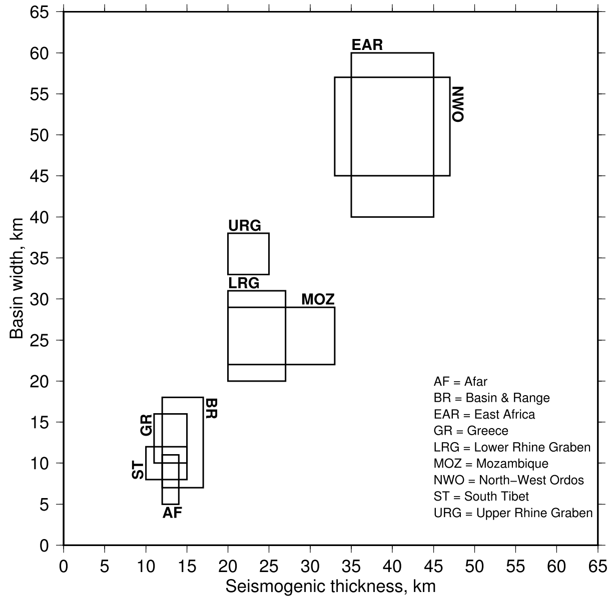

Fig. 2. Relationship between the seismogenic thickness and maximum basin width for regions undergoing present-day extension. Each box represents earthquakes and basins in a different region, described in detail below. The specific areas were selected based on the availability of multiple earthquakes with well-constrained depths that clearly delimit the seismogenic thickness, and clearly-defined extensional basins. GR: the gulfs of Corinth and Evia, and Thessaloniki, Greece (Hatzfeld et al., 1987; Rigo et al., 1996; Hatzfeld et al., 2000); AF: Dobi graben, central Afar (Jacques et al., 1999); ST: central southern Tibet (Liang et al., 2008); BR: Borah Peak region, plus eastern California and western Nevada, Basin and Range, USA (Richins et al., 1987; Ichinose et al., 2003); LRG: Lower Rhine Graben (Vanneste et al., 2013); URG: Upper Rhine Graben (Bonjer, 1997); MOZ: Mozambique (Craig et al., 2011); EAR: western branch of the East African Rift (Craig et al., 2011, and references therein); NWO: north-west margin of Ordos (Cheng et al., 2014).

the faults (i.e. the seismogenic thickness) (e.g. Jackson and White, 1989; Scholz and Contreras, 1998). Deeper faults result in wider basins at the surface. Establishing the modern-day scaling between basin width and seismogenic thickness therefore provides a means to estimate the seismogenic thickness in ancient deformation belts in which basin widths can be observed or inferred. Fig. 2 shows the relationship between maximum basin width and seismogenic thickness in modern-day extensional regions. The relationship between basin width and seismogenic thickness is clearly visible. The boxes encompass the range of maximum basin widths and seismogenic thicknesses for the fault systems in each region, estimated from published mapping, tectonic geomorphology, and local and teleseismic earthquake-source inversions (references given in the figure caption). We only use well-constrained earthquake depths, derived from the modelling of body-waveforms or recordings on dense local networks. The basin width is defined using the subsidence pattern resulting from motion on the presently-active basin-controlling fault (i.e. towards which the sediments in the basin interior dip). Older, inactive faults on the basin margins are not included in the measurements of basin width. As such, each measurement represents the width of basins produced by single, major, faults, and these may be embedded within a region that has experienced prior extension on older faults, or be currently also undergoing extension on other, spatially separated, structures.

Extensional basins formed in the northern UK in the early/mid Carboniferous, which pre-date the Variscan shortening, and are thought to represent back-arc extension before continent-continent collision (e.g. Woodcock and Strachan, 2012). Post-Variscan extensional basins that formed in the Permian and Triassic are thought to be related to post-orogenic collapse and intra-Pangaea rifting (e.g. Woodcock and Strachan, 2012). These pre- and post-Variscan basins show maximum widths of 20–30 km (e.g. the Carboniferous Northumberland Trough, Bowland and North Staffordshire Basins, and southern North Sea, and the Permian and Triassic North Minch and North Lewis Basins and Worcester Graben (Stein and Blundell, 1990; Chadwick et al., 1995; Corfield et al., 1996; Aitkenhead et al., 2002; Waters and Davies, 2006); labelled on Fig. 1). Although some sub-basins show smaller widths, modern-day analogues demonstrate that it is the maximum basin widths in a region that scale with the seismogenic thickness (as plotted on Fig. 2). Basin widths of 20–30 km imply a seismogenic thickness of 15–40 km in the Carboniferous in the UK, based upon Fig. 2. This value is similar to the modern-day value of 20–25 km, based upon the well-constrained depths of recent earthquakes (Baptie, 2010).

Table 1
Parameters used in the calculations.

Adjusted parameters:

Parameter	Minimum value	Maximum value
Seismogenic thickness in lowlands (km)	15	40
Crustal thickness in mountains (km)	55	80
Crustal thickness in lowlands (km)	32	36
Moho temperature in mountains (°C)	600	800
Moho temperature in lowlands (°C)	600	700
Fault strike w.r.t. max. principal stress	45°	90°
Foreland fault dips	45°	70°

Fixed parameters:

Parameter	Value
Density difference from depletion (kg/m^3)	−60
Lithosphere thickness in lowlands (km)	120
Crust density at 0 °C (kg/m^3)	2800
Lithospheric mantle density at 0 °C (kg/m^3)	3330
Thermal expansion co-eff. of crust	3×10^{-5}
Thermal expansion in mantle	Bouhifid et al. (1996)
Mantle potential temperature	1315 °C

4. The forces exerted between mountain ranges and lowlands

It has been previously described how the force exerted between an isostatically-compensated mountain range and the adjacent lowlands can be calculated by summing the lateral differences in the vertical normal stress between the two lithospheric columns (e.g. Artyushkov, 1973; Dalmayrac and Molnar, 1981). It is important to consider density differences resulting from both the thermal structure of the lithosphere and also chemical depletion (e.g. England and Houseman, 1989; Molnar et al., 1993). We have built upon this prior work by calculating the force exerted between a mountain range and an adjacent lowland using a wide range of plausible parameters, in order to estimate the range of possible force magnitudes.

In our calculations we enforce isostatic compensation at the base of the lithosphere, and assume that lithosphere thickness contrasts occur in proportion to crustal thickness contrasts (as has recently shown to be the case in present-day Asia; McKenzie and Priestley, 2016). We vary the crustal thickness in the mountains from 55 to 80 km (the values of all the parameters used in our calculations are given in Table 1). The density reduction caused by the chemical depletion of the lithosphere relative to the asthenosphere is taken to be 60 kg/m^3, based upon geochemical results from Tibet and Iran (McKenzie and Priestley, 2016). The crustal thickness in the lowlands has been varied from 32–36 km, based on receiver functions and seismic experiments in the UK (Davis et al., 2012). We take the lithosphere thickness in the lowlands to be 120 km (McKenzie and Priestley, 2016). We have used densities for the crust and lithospheric mantle at 0 °C of 2800 and 3330 kg/m^3, have used a thermal expansion coefficient of

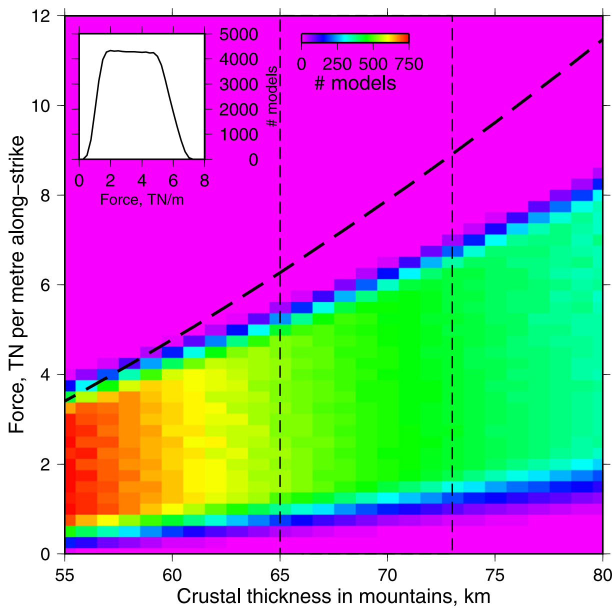

Fig. 3. Distribution of forces exerted between an isostatically-compensated mountain range and the adjacent lowlands, calculated using the range of parameters described in the text. The main figure shows the number of models that predict each value of the force, as a function of the crustal thickness in the mountains. The inset shows the distribution of model results for all values of the crustal thickness in the mountains from 65 to 73 km, marked by the thin dashed lines on the main Figure. The thick dashed line shows the force calculated assuming isostatic compensation at the base of the crust and constant densities of 2800 and 3300 kg/m^3 for the crust and mantle.

3×10^{-5} for the crust, and the expressions of Bouhifid et al. (1996) for the temperature-dependence of density in the mantle (assumed to be dominated by olivine). In the lowlands we assume that the geotherm is in steady-state, which we approximate as linear gradients in the crust and mantle. The temperature at the base of the lithosphere is enforced to be the isentropic temperature at that depth (calculated for a mantle potential temperature of 1315 °C). We have varied the temperature of the Moho in the lowlands between 600 °C and 700 °C, which spans the range commonly suggested for regions with a similar crust and lithosphere thickness to the UK (e.g. Emmerson et al., 2006; Copley et al., 2009). In the mountains we use the shape of the geotherms calculated for southern Tibet by Craig et al. (2012), which take into account the advection of heat caused by underthrusting on the margins of mountain ranges. We scale these geotherms to match the thickness of the crust in the mountains, and to vary the temperature at the Moho between 600 °C and 800 °C (which encompasses inferences from modern-day orogenic belts, based upon thermal models and the distribution of lower-crustal earthquakes (e.g. Craig et al., 2012)).

We have computed the magnitude of the force exerted between the mountains and the lowlands for all combinations of these parameter ranges. Fig. 3 shows the number of models that predict each value of the force, as a function of the crustal thickness in the mountains. The thick dashed black line shows the values obtained by assuming isostatic compensation at the base of the crust, and constant densities for the crust and mantle, which over-estimates the magnitude of the force. Support for our calculations is provided by the independent estimates of the crustal thickness in Tibet (75–80 km, e.g. Mitra et al., 2005), and the force exerted between India and Tibet ($5.5 \pm 1.5 \times 10^{12}$ N/m; Copley et al., 2010), which is in the range predicted by our calculations (Fig. 3). Pressure–temperature estimates from high-grade crustal metamorphic rocks from central Europe imply that the crust in the Variscan mountains was 65–73 km thick (e.g. Kroner and Romer, 2013, and references therein), so Fig. 3 suggests that the force exerted between these mountains and their foreland in the northern UK was 1–6 $\times$ 10^{12} N per metre along-strike. The inset on Fig. 3 shows the relative likelihood of each force value, based upon how many of the combinations of the adjustable parameters result in each estimated value.

5. Fault strength

We can estimate an upper bound on the shear stresses that caused the faults in the Variscan foreland to slip, by assuming that all of the force estimated above is supported by the seismogenic layer. Detailed mapping of the late Carboniferous shortening suggests that the motion was accommodated on structures striking between 45° and 90° from the maximum compression direction (e.g. Corfield et al., 1996; Woodcock and Rickards, 2003; Warr, 2012). In common with modern-day thrusts from regions of reactivated normal-faulting, and mapping of Variscan-age faults in our region of interest, we vary the dip of the faults over the range 45–70° (e.g. Sibson and Xie, 1998; Woodcock and Rickards, 2003). We have conducted calculations to resolve the total force exerted between the mountains and the lowlands onto the foreland faults, using the method of Lamb (2006). This method balances the forces exerted on the wedge of material overlying a fault, and includes both the tectonic stresses and gravity acting on the mass of the rock. Because the seismogenic thickness we estimate is smaller than, or similar to, the crustal thickness, we use only a single fault rheology (rather than using different parameters to represent the crustal and mantle, as done by Lamb, 2006). We use the range of fault strikes and dips described above, along with the range of possible seismogenic thickness estimated above, and the distribution of estimated forces shown in the inset on Fig. 3. Our results for the maximum shear stresses supported by the faults are shown in Fig. 4. The maximum shear stress is most likely to be in the range 10–100 MPa (which encompasses 90% of the models), with a nominal most likely value of 37.5 MPa. The corresponding upper bound on the effective coefficient of friction when these faults slipped is most likely to be in the range 0.02–0.24 (which encompasses 90% of the models), with a nominal most likely value of 0.08. This range is considerably lower than predicted by 'Byerlee's Law' (i.e. 0.6–0.8). For the faults to have slipped in response to the calculated force implies intrinsically weak fault rocks in the reactivated fault zones, high pore fluid pressures, or both. If some of the force transmitted through the Variscan foreland was supported by stresses in the ductile lithosphere, then the faults would be weaker than estimated here. In addition, the above analysis implicitly assumes that the deviatoric stresses in the Variscan Mountains are minor, and that the majority of the force calculated above is supported by the lithosphere in the foreland of the range. However, if significant stresses are supported elsewhere, e.g. by driving the viscous flow of the mountains over the underthrusting foreland, then the faults would be weaker than our estimate.

A striking feature of the late Carboniferous shortening in the northern UK is that many structures were active at an oblique angle to the maximum shortening direction (Fig. 1). The faults that have been studied in detail (e.g. the Dent Fault; Woodcock and Rickards, 2003; Thomas and Woodcock, 2015; labelled on Fig. 1) were pre-existing structures that were re-activated in the late Carboniferous. Fault motion at an oblique angle is less energetically-favourable than motion on an optimally-oriented fault (i.e. perpendicular to the shortening direction, and with a dip that is optimum for the coefficient of friction). We can estimate how much weaker these pre-existing faults must be than optimally oriented, but un-faulted, planes by resolving forces in these two configurations. Specifically, we resolve the total force estimated above onto planes with the dips and orientations observed in the northern UK,

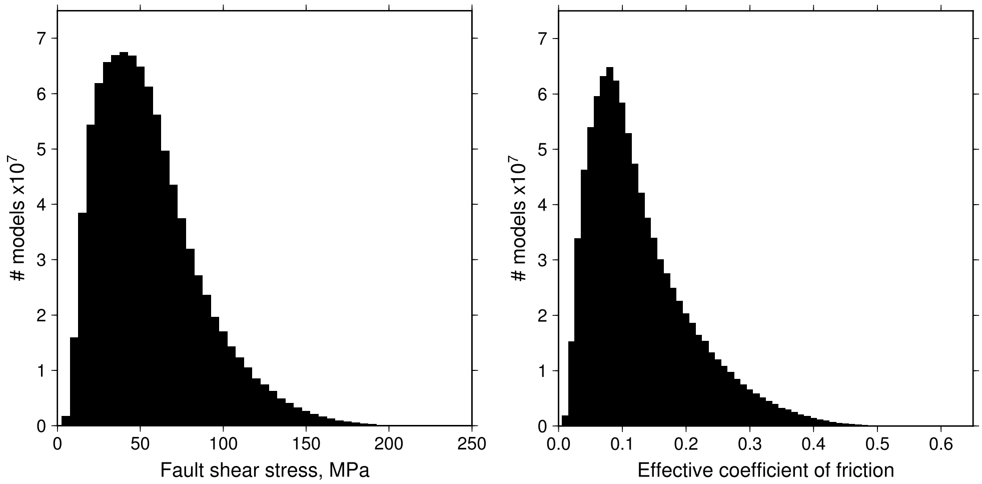

Fig. 4. Estimates of the maximum possible fault shear stress (left) and effective coefficient of friction (right) in the Variscan foreland of the northern UK, based on the ranges of parameters described in the text.

and onto faults that strike perpendicular to the maximum principal stress and dip at angles optimum for their coefficient of friction. The differences in resolved stresses in these two geometries allow us to infer how much weaker pre-existing faults must be than intact rock, in order for reactivation to have occurred, rather than the formation of new faults. We find that the re-activated structures must have an effective coefficient of friction at least 30% lower than intact rock in order for them to have been reactivated, rather than new faults initiating.

6. Conclusions

We have described how to estimate the seismogenic thickness in ancient deformation belts, and have estimated the forces exerted between mountain ranges and lowlands by including thermal and chemical effects on the density. Combining these results for the deformation in the foreland of the Variscan Mountains in the northern UK shows that the faults had a low effective coefficient of friction (i.e. 0.02–0.24), and were at least 30% weaker than unfaulted rock.

Acknowledgements

We thank Simon Lamb and one anonymous reviewer for helpful comments on the manuscript, and the participants in the 2015 Cambridge Earth Sciences field trip to Sedbergh for stimulating discussions. This work forms part of the NERC- and ESRC-funded project ‘Earthquakes without Frontiers’, and was partially supported by the NERC grant ‘Looking Inside the Continents from Space’.

References

Aitkenhead, N., Barclay, W.J., Brandon, A., Chadwick, R.A., Chisholm, M.J.I., Cooper, A.H., Johnson, E.W., 2002. British Regional Geology: The Pennines and Adjacent Areas, 4th edition. HMSO, London.

Allmann, B.P., Shearer, P.M., 2009. Global variations of stress drop for moderate to large earthquakes. J. Geophys. Res. 114. http://dx.doi.org/10.1029/2008JB005821.

Artyushkov, E.V., 1973. Stresses in the lithosphere caused by crustal thickness inhomogeneities. J. Geophys. Res. 78, 7675–7708.

Assumpcao, M., 1992. The regional intraplate stress field in South America. J. Geophys. Res. 97, 11,889–11,903.

Baptie, B., 2010. Seismogenesis and state of stress in the UK. Tectonophysics 482, 150–159.

Bonjer, K-P., 1997. Seismicity pattern and style of seismic faulting at the eastern borderfault of the southern Rhine Graben. Tectonophysics 275, 41–69.

Bouhifid, M.A., Ardrault, D., Fiquet, G., Richet, P., 1996. Thermal expansion of forsterite up to the melting point. Geophys. Res. Lett., 1143–1146.

British Geological Survey, 1996. Tectonic Map of Britain, Ireland and Adjacent Areas. British Geological Survey, Nottingham.

Brudy, M., Zoback, M.D., Fuchs, K., Rummel, F., Baumgartner, J., 1997. Estimation of the complete stress tensor to 8 km depth in the KTB scientific drill holes: implications for crustal strength. J. Geophys. Res. 102, 18,453–18,475.

Byerlee, J., 1978. Friction of rocks. Pure Appl. Geophys. 116, 615–626.

Chadwick, R.A., Holliday, D.W., Holloway, S., Hulbert, A.G., 1995. The Structure and Evolution of the Northumberland–Solway Basin and Adjacent Areas: Subsurface Memoir. British Geological Survey, HMSO, London.

Cheng, B., Cheng, S., Zhang, G., Zhao, D., 2014. Seismic structure of the Helan–Liupan–Ordos western margin tectonic belt in north-central China and its geodynamic implications. J. Asian Earth Sci. 87, 141–156.

Collettini, C., Sibson, R.H., 2001. Normal faults, normal friction? Geology 29, 927–930.

Copley, A., Boait, F., Hollingsworth, J., Jackson, J., McKenzie, D., 2009. Sub-parallel thrust and normal faulting in Albania and the role of gravitational potential energy and rheology contrasts in mountain belts. J. Geophys. Res. 114. http://dx.doi.org/10.1029/2008JB005931.

Copley, A., Avouac, J-P., Royer, J-Y., 2010. The India–Asia collision and the Cenozoic slowdown of the Indian plate: implications for the forces driving plate motions. J. Geophys. Res. 115. http://dx.doi.org/10.1029/2009JB006634.

Copley, A., Avouac, J-P., Hollingsworth, J., Leprince, S., 2011. The 2001 Mw 7.6 Bhuj earthquake, low fault friction, and the crustal support of plate driving forces in India. J. Geophys. Res. 116. http://dx.doi.org/10.1029/2010JB008137.

Corfield, S.M., Gawthorpe, R.L., Gage, M., Fraser, A.J., Besley, B.M., 1996. Inversion tectonics of the Variscan foreland of the British Isles. J. Geol. Soc. 153, 17–32.

Craig, T., Copley, A., Jackson, J., 2012. Thermal and tectonic consequences of India underthrusting Tibet. Earth Planet. Sci. Lett. 353–354, 231–239.

Craig, T., Copley, A., Middleton, T., 2014. Constraining fault friction in oceanic lithosphere using the dip angles of newly-formed faults at outer rises. Earth Planet. Sci. Lett. 392, 94–99.

Craig, T.J., Jackson, J.A., Priestley, K., McKenzie, D., 2011. Earthquake distribution patterns in Africa: their relationship to variations in lithospheric and geological structure, and their rheological implications. Geophys. J. Int. 185, 403–434.

Dalmayrac, B., Molnar, P., 1981. Parallel thrust and normal faulting in Peru and constraints on the state of stress. Earth Planet. Sci. Lett. 55, 473–481.

Davis, M.W., White, N.J., Priestley, K.F., Baptie, B.J., Tilmann, F.J., 2012. Crustal structure of the British Isles and its epeiogenic consequences. Geophys. J. Int. 190, 705–725.

Emmerson, B., Jackson, J., McKenzie, D., Priestley, K., 2006. Seismicity, structure, and rheology of the lithopshere in the Lake Baikal region. Geophys. J. Int. 167, 1233–1272.

England, P., Houseman, G., 1989. Extension during continental convergence, with application to the Tibetan plateau. J. Geophys. Res. 94, 17561–17579.

Hatzfeld, D., Christodoulou, A.A., Scordilis, E.M., Panagiotopoulos, D., Hatzidimitriou, P.M., 1987. A microearthquake study of the Mygdonian graben (northern Greece). Earth Planet. Sci. Lett. 81, 379–396.

Hatzfeld, D., Karakostas, V., Ziazia, M., Kassaras, I., Papadimitriou, E., Makropoulos, K., Voulgaris, N., Papaioannou, C., 2000. Microsesmicity and faulting geometry in the Gulf of Corinth (Greece). Geophys. J. Int. 141, 438–456.

Ichinose, G.A., Anderson, J.G., Smith, K.G., Zeng, Y., 2003. Source parameters of Eastern California and Western Nevada earthquakes from regional moment tensor inversion. Bull. Seismol. Soc. Am. 93, 61–84.

Jackson, J.A., White, N.J., 1989. Normal faulting in the upper continental crust: observations from regions of active extension. J. Struct. Geol. 11, 15–36.

Jacques, E., Ruegg, J.C., Lepine, J.C., Tapponnier, P., King, G.C.P., Omar, A., 1999. Relocation of M>2 events of the 1989 Dobi seismic sequence in Afar: evidence for earthquake migration. Geophys. J. Int. 138, 447–469.

Kanamori, H., Anderson, D.L., 1975. Theoretical basis of some empirical relations in seismology. Bull. Seismol. Soc. Am. 65, 1073–1095.

Kroner, U., Romer, R.L., 2013. Two plates – many subduction zones: the Variscan orogeny reconsidered. Gondwana Res. 24, 298–329.

Lamb, S., 2006. Shear stresses on megathrusts: implications for mountain building behind subduction zones. J. Geophys. Res. 111. http://dx.doi.org/10.1029/2005JB003916.

Liang, X., Zhou, S., Chen, Y.J., Jin, G., Xiao, L., Liu, P., Fu, Y., Tang, Y., Lou, X., Ning, J., 2008. Earthquake distribution in southern Tibet and its tectonic implications. J. Geophys. Res. 113. http://dx.doi.org/10.1029/2007JB005101.

Lockner, D.A., Morrow, C., Moore, D., Hickman, S., 2011. Low strength of deep San Andreas fault gouge from SAFOD core. Nature 472, 82–85.

McKenzie, D., Priestley, K., 2016. Speculations on the formation of cratons and cratonic basins. Earth Planet. Sci. Lett. 435, 94–104.

Middleton, T.A., Copley, A., 2014. Constraining fault friction by re-examining earthquake nodal plane dips. Geophys. J. Int. 196, 671–680.

Mitra, S., Priestley, K., Bhattacharyya, A.K., Gaur, V.K., 2005. Crustal structure and earthquake focal depths beneath northeastern India and southern Tibet. Geophys. J. Int. 160, 227–248.

Molnar, P., England, P., Martinod, J., 1993. Mantle dynamics, uplift of the Tibetan plateau, and the Indian monsoon. Rev. Geophys. 31, 357–396.

Richins, W.D., Pechmann, J.C., Smith, R.B., Langer, C.J., Goter, S.K., Zollweg, J.E., King, J.J., 1987. The 1983 Borah Peak, Idaho, earthquake and its aftershocks. Bull. Seismol. Soc. Am. 77, 694–723.

Rigo, A., Lyon-Caen, H., Armijo, R., Deschamps, A., Hatzfeld, D., Makropoulos, K., Papadimitriou, P., Kassaras, I., 1996. A microseismic study in the Gulf of Corinth (Greece): implications for large-scale normal faulting mechanisms. Geophys. J. Int. 126, 663–688.

Scholz, C.H., Contreras, J.C., 1998. Mechanics of continental rift architecture. Geology 26, 967–970.

Sibson, R.H., Xie, G., 1998. Dip range for intracontinental reverse fault ruptures: truth not stranger than friction? Bull. Seismol. Soc. Am. 88, 1014–1022.

Stein, A.M., Blundell, D.J., 1990. Geological inheritance and crustal dynamics of the northwest Scottish continental shelf. Tectonophysics 173, 455–467.

Thomas, C.W., Woodcock, N.H., 2015. The kinematic linkage of the Dent, Craven, and related faults of Northern England. Proc. Yorks. Geol. Soc. 60, 258–274.

Townend, J., Zoback, M.D., 2000. How faulting keeps the crust strong. Geology 28, 399–402.

Ujiie, K., Tanaka, H., Saito, T., Tsutsumi, A., Mori, J.J., Kameda, J., Brodsky, E.E., Chester, F.M., Eguchi, N., Toczko, S., 2013. Expedition 343, and 343T scientists. Low coseismic shear stress on the Tohoku-Oki megathrust determined from laboratory experiments. Science 342, 1211–1214.

Vanneste, K., Camelbeeck, T., Verbeek, K., 2013. A model of composite seismic sources for the Lower Rhine Graben, northwest Europe. Bull. Seismol. Soc. Am. 103, 984–1007.

Warr, L.N., 2012. The Varican orogeny: the welding of Pangaea. In: Woodcock, N., Strachan, R. (Eds.), Geological History of Britain and Ireland. Wiley–Blackwell.

Waters, C.N., Davies, S.J., 2006. Carboniferous: extensional basins, advancing deltas and coal swamps. In: Brenchley, P.J., Rawson, P.F. (Eds.), The Geology of England and Wales, 2nd edition. The Geological Society, London.

Woodcock, N.H., Rickards, B., 2003. Transpressive duplex and flower structure: dent fault system, NW England. J. Struct. Geol. 25, 1981–1992.

Woodcock, N., Strachan, R., 2012. Geological History of Britain and Ireland. Wiley–Blackwell.